Journal of Coordination Chemistry

ISSN: 0095-8972 (Print) 1029-0389 (Online) Journal homepage: http://www.tandfonline.com/loi/gcoo20

Characterization and oxidative addition reactions for iridium cod complexes

W. Purcell, J. Conradie, S. Kumar & J. A. Venter

To cite this article: W. Purcell, J. Conradie, S. Kumar & J. A. Venter (2017) Characterization and oxidative addition reactions for iridium cod complexes, Journal of Coordination Chemistry, 70:1, 10-24, DOI: 10.1080/00958972.2016.1261402

To link to this article: http://dx.doi.org/10.1080/00958972.2016.1261402

Accepted author version posted online: 15 Nov 2016.
Published online: 29 Nov 2016.

JOURNAL OF COORDINATION CHEMISTRY, 2017
VOL. 70, NO. 1, 10–24
http://dx.doi.org/10.1080/00958972.2016.1261402

Taylor & Francis
Taylor & Francis Group

Characterization and oxidative addition reactions for iridium cod complexes

W. Purcell, J. Conradie, S. Kumar and J. A. Venter

Department of Chemistry, University of the Free State, Bloemfontein, South Africa

ABSTRACT

Three different [Ir(LL')(cod)] complexes (LL' = N-aryl-N-nitrosohydroxylaminato) *(cupf)*, trifluoroacetylacetonato *(tfaa)*, and (methyl 2-(methylamino)-1-cyclopentene-1-dithiocarboxylato-κN,κS) (*macsm*)) were synthesized, characterized, and their rates of oxidative addition with methyl iodide were determined. Formation of an isosbestic point during the oxidative addition of methyl iodide with the complexes containing tfaa and cupf as bidentate ligands indicated formation of only one product, while an increase in absorbance maximum observed for macsm confirms that the same reaction between the complex and methyl iodide occurs. Kinetic results for all complexes, except [Ir(tfaa)(cod)], showed simple second-order kinetics with a zero intercept (within experimental error). Rates of oxidative addition for bidentate ligands in acetonitrile showed an increase of an order of magnitude with a change in the type of bidentate ligands. Computational chemistry using density functional theory calculations showed that the oxidative addition reaction proceeds through a "linear" transition state with the methyl iodide unit tilted towards the LL'-bidentate ligand.

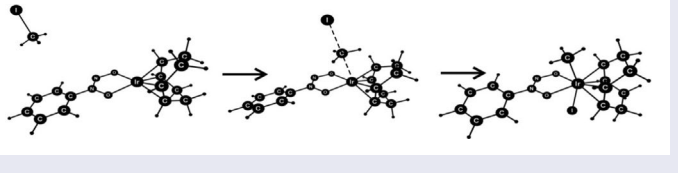

ARTICLE HISTORY
Received 26 July 2016
Accepted 3 October 2016

KEYWORDS
Iridium(I); bidentate ligands; cyclooctadiene; oxidative addition; methyl iodide

1. Introduction

The use of iridium complexes as catalysts in the synthesis of large-scale organic compounds are relatively new compared to other metals. $[IrI_2(CO)_2]^-$ is used by British Petroleum in its well-known Cativa process [1–4] for the production of acetic acid from methanol, while an Ir-xyliphos complex is used by Novartis [5–7] to synthesize the herbicide (S)-metolachlor. Another very important iridium catalyst is the Crabtree catalyst ($[Ir(cod)(PCy_3)(py)][PF_6]$) [8, 9], which showed a 100 times increase in hydrogenation activity compared to the Wilkinson catalyst ($[Rh(PPh_3)_3Cl]$) and even allowed for hydrogenation of tri- and tetra-substituted

CONTACT W. Purcell purcellw@ufs.ac.za

alkenes. The complex also showed excellent stereoselectivity in reduction of exocyclic methylene groups compared to more traditional catalysts such as [Rh(ndb)(dppb)]BF_4 (dppb = 1,4-bis(diphenylphosphino)butane), [Rh(PPh_3)$_3$Cl], and Pd/C [10].

The iridium(I) cyclooctadiene dimer [Ir(cod)Cl]$_2$ is prepared with reaction between $Na_2[IrCl_6]\cdot 6H_2O$ or $H_2[IrCl_6]\cdot 6H_2O$ and cycloocta-1,5-diene [11, 12]. This iridium organometallic complex can undergo bridge-splitting and cod substitution reactions to synthesize a number of new iridium organometallic complexes or the complex can also facilitate oxidative addition reactions. [Ir(cod){($P(OPh)_3$}$_2$]$^+$ [13] is an example of a product formed after a bridge-splitting reaction while isolation of [IrCl($CO)_2$(PPh_3)] [12] is an example of a cod substitution reaction. Examples of oxidative addition reactions include the direct reaction of HCl or HBr to produce [Ir(cod)HCl_2]$_2$ [14] and [Ir(cod)HBr_2]$_2$ [15].

Oxidative addition is a key reaction in the cyclic catalytic conversion of methanol to acetic acid in both the Monsanto and the Cativa processes [16]. This reaction is followed by methyl migration, reductive elimination of the acetyl iodide, and the final step is its reaction with water to produce acetic acid and the original metal complex is regenerated. The rate and the mechanism of the oxidative addition step for both Rh and Ir square planar complexes are influenced by electronic (type, ring size and atom combination of bidendate ligands), steric (cone angle of phosphine ligands), and solvent effects. The spontaneous methyl migration step observed [17, 18] for most of the complexes complicate the kinetic study of these reactions with the formation of different isomers in solution, the presence of equilibria and solvent-assisted reaction pathways [19].

Kinetic study of the oxidative addition reactions of [Ir(L,L′)(cod)] complexes would simplify the overall reaction with no CO insertion taking place, the formation of only one isomer and simplified mechanisms with possible zero intercepts. A kinetic study of the oxidative addition reaction between [Ir(sasac)(cod)] and CH_3I in different solvents produces simplified kinetics [20].

In this study, three different iridium(I) cod complexes [Ir(LL′)(cod)] were synthesized, with LL′ = N-aryl-N-nitrosohydroxoylaminato *(cupf))*, trifluoroacetylacetonato *(tfaa)*, and (methyl 2-(methylamino)-1-cyclopentene-1-dithiocarboxylato-κN,κS) (*macsm*) (see scheme 1), to determine the electronic influence of different donor ligands on the oxidative addition step for these complexes. A computational chemistry study on the geometries and energies of the reactants, transition state and possible products of the [Ir(LL′)(cod)] + CH_3I reaction, shed further light on the oxidative addition process.

2. Experimental

2.1. General considerations

Unless otherwise stated, all chemicals were reagent grade and used without purification and all preparations were carried out in air. The bidendate ligands cupf (N-aryl-N-nitrosohydroxylaminato) and tfaa (1,1,1-trifluoropentane-2,4-dione) were commercially obtained and used without purification. IR spectra were recorded with a Hitachi 270–50 spectrophotometer while the NMR spectra (TMS as internal standard) were obtained at 293 K on a Bruker 600 MHz spectrometer. The methyl iodide was stabilized by silver foil to prevent decomposition and used in a well-ventilated fume cupboard. The CHN analyses were performed on a LECO Truspec micro-analyzer, while the iridium analysis was performed on a Shimadzu ICPS-7510 ICP-OES sequential plasma spectrometer.

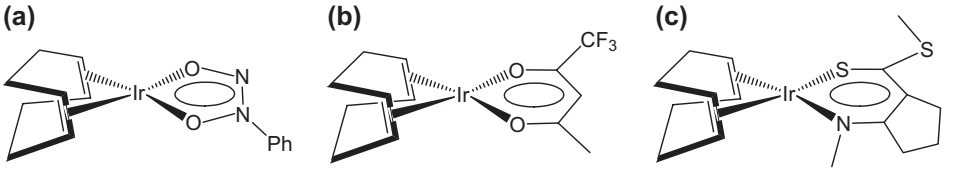

Scheme 1. Different iridium(I) cod complexes synthesized in the study: (a) [Ir(cupf)(cod)], (b) [Ir(tfaa)(cod)] and (c) [Ir(macsm)(cod)].

The UV/Visible spectra and kinetic runs were performed on a Hitachi 150–20 UV/Visible spectrophotometer in a thermostatically controlled holder (0.1 °C), which has a capacity of 6 cells. The solvents used for the kinetic runs were all purified and dried using the prescribed methods [21]. All the complexes were tested for stability in the different solvents prior to the kinetic runs. Typical experimental conditions were [M(cod)(LL′)] = 5.0×10^{-4} M, and [CH_3I] varied between 0.075 and 0.75 M, which ensured good pseudo-first-order kinetics. The observed first-order rate constants (k_{obs}) were calculated for at least two half-lives from the above plots using the equation $A_t = A_\infty + (A_0 - A_\infty)e^{(-kobs*t)}$ with A_0, A_t, and A_∞ the absorbance at time 0, t and infinity, respectively, using a nonlinear least squares program [22].

2.2. Synthesis

Slight variations of previously published synthetic routes [23] were introduced in the preparation of macsm.

2.2.1. (Methyl 2-(methylamino)-1-cyclopentene-1-dithiocarboxylato-κN,κS) (macsm) [23]

Cyclopentanone (4.2 g, 0.05 mol) was mixed with an aqueous methylamine (31 g, 0.2 mol) solution. The mixture was cooled to 5 °C and stirred for 120 min after which carbon disulfide (4.6 g, 0.06 mol) was gradually introduced and stirred for another 120 min. The yellow precipitate was removed by filtration and washed with water. The dried product was added to 8-mL concentrated acetic acid and heated to 50 °C for a few minutes. The mixture was cooled to room temperature and 20 mL of water was introduced. The yellow solid was then removed by filtration, washed with water and dried, yield 25%. About 3.6 g of this product was dissolved in 6-mL 40% aqueous methyl amine solution, 30-mL methanol was added and refluxed for 180 min. The volume of the solution was reduced under reduced pressure, the residue added to 70 mL of water and the precipitate removed by precipitation. Hydrochloric acid (10%) was added to the filtrate, which resulted in formation of a yellow solid product. About 1 g of this product was dissolved in 5 mL of 6 M NaOH, an excess (≈1 mL) of methyl iodide was slowly added with constant stirring for 2 h resulting in formation of a yellow solid product, which was filtered and dried. Yield 58%, M.P 127–129 °C, Elemental analysis for $C_8H_{13}NS_2$ (Mr = 187.05): Found C, 51.34; H, 6.89; N, 7.32; S, 34.10%; Calcd C, 51.29; H, 6.99; N, 7.48; S, 34.23%; IR spectra: ν = 2971 (C–H, str), 1598 (C=N), 613 (C–S) cm^{-1}, ^{1}H NMR (600 MHz), $CDCl_3$, 20 °C: δ 1.89 (2H, m), 2.59 (3H, s), 2.69 (2H, m), 2.82 (2H, m), 3.07 (3H, s) ppm. ^{13}C NMR (600 MHz), $CDCl_3$, 20 °C: δ 16.6, 20.6, 31.4, 33.0, 33.4, 118.3, 170.1, 197.3.

2.2.2. (η^4-1,5-Cyclooctadiene-N-aryl-N-nitrosohydroxylaminato)iridium(I), [Ir(cupf)(cod)]

[IrCl(cod)]$_2$ (0.5 g, 0.9 mmol) was dissolved in 20-mL dimethyl formamide (DMF). Cupf (0.45 g, 2.5 mmol) was dissolved in 6-mL DMF and slowly added while continuously stirring the solution. The color changed from yellow to bright red. Water was added dropwise and a yellow product precipitated from the solution, which was removed with centrifuging. The product was then redissolved in minimum acetone and re-precipitated with the addition of water and isolated with centrifuging. The yellow product was washed with water and dried over P_2O_5 in a vacuum desiccator. Yield: 68%; IR spectra: v = 3080 (Ar-C-H, str), 749 (=C–H bending), 1455 (N–N=O) cm^{-1}; MS; *m/z* 437.23 [M]$^+$, 438.28 [M + H]$^+$; Elemental analysis for $C_{14}H_{17}IrN_2O_2$ (Mr = 437.52): Found C, 38.21; H, 3.89; N, 6.37%; Calcd C, 38.43; H, 3.92; N, 6.40%; ^{1}H NMR (600 MHz), $CDCl_3$, 20 °C: δ 1.74 (4H, m), 2.25 (4H, m), 4.24 (2H, t), 4.30 (2H, t), 7.47 (1H, m), 7.49, (2H, m), 7.98 (2H, m), ppm. ^{13}C NMR (600 MHz), $CDCl_3$, 20 °C: δ 30.8, 31.0, 57.4, 58.4, 121.1, 129.4, 130.7, 138.2.

2.2.3. (η^4–1,5-Cyclooctadiene)(iodo)(methyl)(N-aryl-N-nitrosohydroxylaminato) iridium(III), [Ir(cupf)(cod)(CH_3)I]

An excess of CH_3I (10 mL) and [Ir(cupf)(cod)] (0.2 g, 0.47 mmol) was mixed in 2 mL acetone. The solution was sealed for 60 min. The seal was removed and the solution was concentrated in a vacuum desiccator. The concentrated solution was kept at −10 °C and an orange precipitate was isolated from the solution. Yield: 63%; IR spectra: v = 3054 (Ar–C–H, str), 766 (=C–H bending), 1460 (N-N=O) cm^{-1}. MS; *m/z* 579.50 [M]$^+$, 580.01 [M + H]$^+$; Elemental analysis for $C_{15}H_{20}IIrN_2O_2$ (Mr = 579.45): Found C, 31.64; H, 3.46; N, 4.79%; Calcd C, 31.09; H, 3.48; N, 4.83%; ^{1}H NMR (600 MHz), $CDCl_3$, 20 °C; δ 1.39 (1H, m), 1.48 (1H, m), 1.70 (1H, m), 2.40 (1H, m), 2.47 (1H, m,), 2.49 (1H, m), 2.49 (1H, m), 2.58(1H, m), 3.01 (3H, s), 4.39 (1H, m), 4.61 (1H, m), 4.72 (1H, m), 5.40 (1H, m), 7.48 (1H, m), 7.52 (2H, m), 8.06 (2H, m). ^{13}C NMR (600 MHz), $CDCl_3$, 20 °C; δ 8.6, 28.8, 29.0, 30.2, 33.7, 77.2, 79.0, 95.2, 97.1, 121.8, 129.4, 130.7, 139.1.

2.2.4. (η^4–1,5-Cyclooctadiene-trifluoroacatylacetonato)iridium(I), [Ir(tfaa)(cod)]

The procedure for synthesis of [Ir(tfaa)(cod)] was identical to that of [Ir(cupf)(cod)]. Yield: 61%; IR spectra: v = 2945 (C–H str), 774 (=C–H bending), 1302 (C–F), 1142 (C–O) cm^{-1}; MS; *m/z* 453.16 [M]$^+$, 454.13 [M + H]$^+$; Elemental analysis for $C_{13}H_{16}F_3IrO_2$ (Mr = 453.5): Found C, 34.01; H, 3.84%; Calcd C, 34.39; H, 3.56%; ^{1}H NMR, (600 MHz), $CDCl_3$, 20 °C: δ 1.60 (4H, m), 2.07 (3H, s), 2.19 (4H, m), 4.10 (2H, m), 4.14 (2H, m), 5.87 (1H, s) ppm. ^{13}C NMR (600 MHz), $CDCl_3$, 20 °C: δ 29.03, 31.03, 31.10, 60.34, 61.13, 97.47, 118.1 167.54, 194.31.

2.2.5. (η^4–1,5-Cyclooctadiene)(iodo)(methyl)(trifluoroacatylacetonato)iridium(III), [Ir(tfaa)(cod)(CH_3)I]

The procedure for the synthesis of [Ir(tfaa)(cod)(CH_3)I] was identical to that of [Ir(cupf)(cod)(CH_3)I]. Yield: 60%; IR spectra: v = 3014 (C–H, str), 801(=C–H bending), 1296 (C–F), 1146 (C–O) cm^{-1}; MS; *m/z* 597.25 [M]$^+$, 598.21 [M + H]$^+$; Elemental analysis for $C_{14}H_{19}F_3IrIO_2$ (595.42): Found C, 28.07; H, 3.37%; Calcd C, 28.24; H, 3.22%; ^{1}H NMR (600 MHz), $CDCl_3$, 20 °C: δ 1.92 (2H, m), δ 2.16 (3H, s), 2.17 (2H, m), 2.23 (3H, s), 2.63 (2H, m), 3.09 (2H, m), 4.29 (2H, m), 5.27 (2H, m), 5.97 (1H, s). ^{13}C NMR (600 MHz), $CDCl_3$, 20 °C: δ 17.2, 28.4, 28.5, 29.3, 33.1, 33.2, 99.3, 116.2, 167.1 194.9.

2.2.6. (η^4–1,5-Cyclooctadiene-methyl-2-(methylamino)-1-cyclopentene-1-dithiocarboxylato)iridium(I), [Ir(macsm)(cod)]

The procedure for the synthesis of [Ir(macsm)(cod)] was identical to that of [Ir(cupf)(cod)]. Yield: 64%; IR spectra: v = 2974 (C–H, str), v = 1602 (C=N), 792 (=C–H bending), 621 (C–S) cm^{-1}; MS; m/z 486.25 $[M]^+$, 487.26 $[M + H]^+$; Elemental analysis for Ir(macsm)(cod)], $C_{16}H_{24}IrNS_2$ (486.73)): Found C, 39.20; H, 5.01; N,2.75; S, 12.99%; Calcd C, 39.40; H, 5.17; N, 2.87; S, 13.15%; ^{1}H NMR (600 MHz), $CDCl_3$, 20 °C; δ 1.83 (2H, m), 1.91 (2H, m), 1.97 (2H, m), 2.17 (2H, m), 2.38 (2H, m), 2.58 (3H, s), 2.76 (2H, m), 2.86 (2H, m), 3.49 (3H, s), 4.07 (2H, m), 4.14 (2H, m). ^{13}C NMR (600 MHz), $CDCl_3$, 20 °C; δ 17.82, 21.05, 29.97, 32.08, 34.54, 38.67, 44.18, 59.17, 69.84, 125.74, 160.53, 172.88.

2.2.7. (η^4–1,5-Cyclooctadiene-methyl-2-(methylamino)-1-cyclopentene-1-dithiocarboxylato)(iodo)(methyl)iridium(III), [Ir(macsm)(cod)CH_3I]

The procedure for the synthesis of [Ir(macsm)(cod)(CH_3)I] was identical to that of [Ir(cupf)(cod)(CH_3)I]. Yield: 64%; IR spectra: v = 2927 (C–H, str), 1640 (C=N), 796 (=C–H bending), 636 (C–S) cm^{-1}; MS; m/z 628.18 $[M]^+$, 629.19 $[M + H]^+$; Elemental analysis for $C_{17}H_{27}IrINS_2$ (628.66): Found C, 32.21; H, 4.40; N, 2.30; S, 10.02%; Calcd C, 32.43; H, 4.48; N, 2.22; S, 10.18%; ^{1}H NMR (600 MHz), $CDCl_3$, 20 °C; δ 1.73 (1H, m), 1.83 (3H, s), 1.85 (1H, m), 1.97 (1H, m), 2.17 (1H, m), 2.23 (1H, m), 2.46 (3H, s), 2.50 (1H,m), 2.60 (1H, m), 2.63 (1H, m), 2.70 (1H, m), 2.75 (1H, m), 2.78 (1H, m), 2.83 (1H, m), 3.08 (1H, m), 3.23 (3H, s), 3.30 (1H, m), 4.31 (1H, m), 4.59 (1H, m), 4.98 (1H, m), 5.63 (1H, m). ^{13}C NMR (600 MHz), $CDCl_3$, 20 °C; δ 6.1, 17.0, 20.8, 27.0, 29.5, 31.6, 34.1, 35.3, 38.2, 45.2, 80.1, 80.8, 92.0, 94.1, 122.6, 157.1, 171.6.

2.3. Kinetics

The UV/visible spectrum of the oxidative addition reactions of [Ir(tfaa)(cod)] and [Ir(cupf)(cod)] with methyl iodide in acetonitrile showed one reaction with formation of an isosbestic point at 365 nm (figure 1(a)) and 375 nm, respectively (figure 1(b)), while the same reaction between [Ir(macsm)(cod)] and methyl iodide (figure 1(c)) showed only an increase in absorption over the whole spectrum.

Results from the initial methyl iodide concentration variations in acetonitrile indicated linear relationships for all three complexes with an intercept close to zero as illustrated by

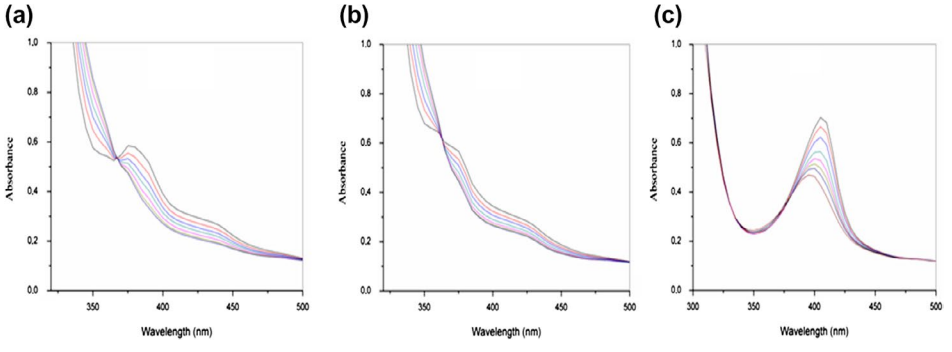

Figure 1. Spectral change with the addition of CH_3I to (a) [Ir(tfaa)(cod)], (b) [Ir(cupf)(cod)] and (c) [Ir(macsm)(cod)] in acetonitrile at 298 K and 10 min intervals, [CH_3I] = .2 M.

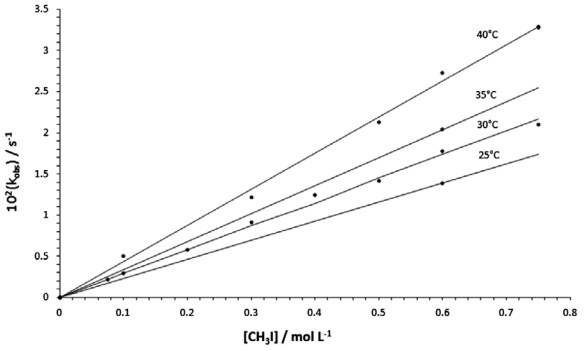

Figure 2. k_{obs} *vs.* [CH_3I] in acetonitrile at different temperatures for the reaction [Ir(macsm)(cod)] + CH_3I, [Ir(macsm)(cod)] = 5.0×10^{-4} mol L^{-1}.

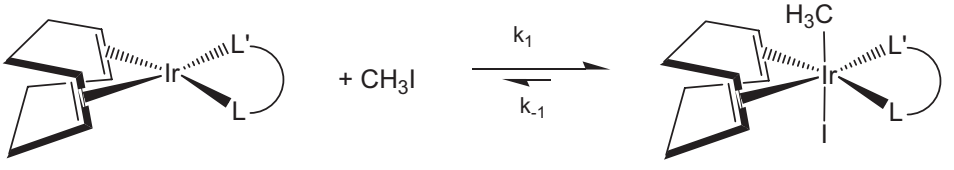

Scheme 2. Proposed reactions between [Ir(LL')(cod)] and CH_3I (LL' = cupf, tfaa and macsm).

Table 1. Summary of the kinetic data and activation parameters for the oxidative addition reactions of different [Ir(LL)(cod] complexes and CH_3I in acetonitrile at 25° C.

Complex	k_1 (10^3) ($M^{-1}s^{-1}$)	k_{-1}(10^4) (s^{-1})	$\Delta H^{\neq}$ (kJ mol^{-1})	$\Delta S^{\neq}$ (J K^{-1} mol^{-1})
[Ir(cupf)(cod)]	2.98(4)	1.1(5)	31(4)*	−189(15)*
			92(28)**	−3(3)**
[Ir(tfaa)(cod)]	4.4(2)	–	37(2)	−166(7)
[Ir(macsm)(cod)]	2.84(7)	–	30(2)	−174(7)

* Forward reaction.
** Reverse reaction.

oxidative addition of [Ir(macsm)(cod)] and CH_3I in acetone (figure 2). These results led to a very simple reaction mechanism (scheme 2).

The rate law for this reversible reaction is given by equation 1:

$$R = k_1[\mathrm{Ir(LL')(cod)}][\mathrm{CH_3\,I}] - k_{-1}[\mathrm{Ir(LL')(cod)(CH_3)I}] \quad (1)$$

The observed rate constant after integration and using pseudo-first-order conditions is given by equation 2:

$$k_{obs} = k_1[CH_3I] + k_{-1} \quad (2)$$

A summary of the calculated rate constants as well as activation parameters is given in table 1. These values indicate that the k_{-1} values for the different complexes, with the exception of [Ir(cupf)(cod)] in acetonitrile, are all zero within experimental error.

2.4. Computational study

Calculations were done using the density functional theory (DFT) as implemented in the Amsterdam Density Functional 2013 program system [24]. The PW91 (Perdew-Wang 1991)

[25] GGA (Generalized Gradient Approximation) functional, a Slater-type TZP (triple-ζ plus polarization) basis set, a fine mesh for numerical integration, and full geometry optimizations with tight convergence criteria were used. All structures were calculated as singlet states ($S = 0$) and the geometry optimizations were all symmetry-unconstrained. Scalar relativistic and solvent effects were taken into account using the ZORA [26] (Zero-Order Regular Approximation) formalism and the COSMO (Conductor like Screening Model) model of solvation [27], respectively. The type of cavity used for the solvent effects was Esurf [28] and the solvent used was acetonitrile ($\varepsilon_0 = 37.5$) to match the experimental conditions. All transition states and minima were confirmed with frequency analyses. Zero-point energy and thermal corrections (vibrational, rotational and translational) were made to the electronic energies in the calculation of the thermodynamic parameters. Enthalpies (H) and Gibbs free energies (G) were calculated from:

$$U = E_{el} + E_{IE} \tag{3}$$

$$H = U + RT(\text{for gas phase}); \text{or } H = U(\text{in solution}) \tag{4}$$

$$G = H - TS \tag{5}$$

where U = the total energy, E_{el} = total electronic energy, and E_{IE} = internal energy (sum of vibrational, rotational, translational energies including the zero-point energy correction), R = ideal gas constant, T = temperature and S = entropy. The entropy (S) was calculated from the temperature-dependent partition function in ADF at 298.15 K.

3. Results and discussion

3.1. Synthesis

All six iridium complexes were synthesized and characterized by ^{1}H and ^{13}C NMR, microanalysis and infrared spectroscopy. The ^{1}H NMR data are summarized in table 2. The eight cod methylene protons for all the isolated complexes are observed between δ 1.39 and 3.09, while the protons in two of the three isolated oxidative addition products are shifted downfield. The four cod double bond protons in the starting compounds appear only as two peaks, suggesting similar chemical environments on each side of the square planar compound, but these peaks shift downfield and are split into four peaks for two of the three oxidative addition products. This confirms the difference in the chemical environment above and below the plane, as well as on either side of the oxidative addition product after coordination of CH_3 and I to the metal center. The absence of splitting in the tfaa complex suggests insignificant changes in the chemical environment above and below the plane after oxidative addition. The methyl groups in the oxidative addition products appear between δ 1.83 and 3.01 ppm confirming coordination of methyl iodide to the metal center in the different isolated oxidative addition products.

The ^{13}C NMR of [Ir(cupf)(cod)(CH_3)I] indicated the presence of 13 carbons with the aliphatic carbons assigned between 28.8 and 97.1 ppm and the aromatic carbons between 121.1 and 139.1 ppm. The APT experiment (ATP = Attached Proton test) for the same complex indicates four carbons with an uneven number of protons (negative mode) and nine carbons with an

Table 2. Summary of the ^{1}H spectra of all the isolated complexes.

	^{1}H spectra/δ ppm				
Complex	Methylene protons (cod)	Double bond protons (cod)	Aromatic proton	Methyl group	Methine
[Ir(cupf)(cod)]	1.74–2.25	4.24, 4.30	7.47 – 7.98		
[Ir(cupf)(cod)(CH_3)I]	1.39–2.58	4.39, 4.61, 4.72, 5.40	7.48 – 8.08	**3.01**	
Ir(tfaa)(cod)]	1.60–2.19	4.10, 4.14		2.07	5.87
[Ir(tfaa)(cod)(CH_3)I]	1.92–3.09	4.29, 5.27		2.16, **2.23**	5.97
[Ir(macsm)(cod)]	1.96–2.40 1.83–2.86*	4.07, 4.14		2.58, 3.49	
[Ir(macsm)(cod)(CH_3)I]	1.97–3.08 1.73–2.83*	4.31, 4.59, 4.98, 5.63		**1.83**, 2.46, 3.23	

*Cyclopentane ring.
Bold: Methyl group after oxidative addition.

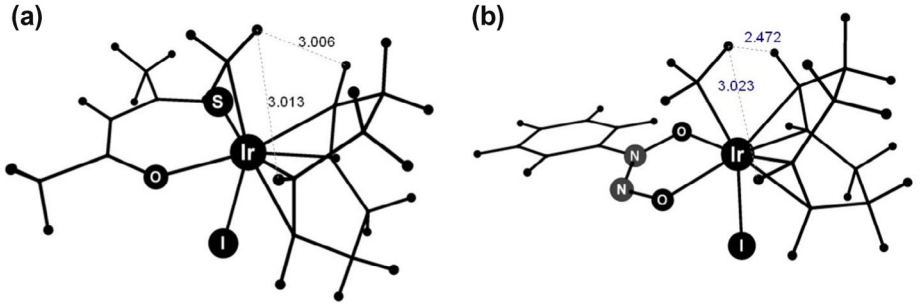

Figure 3. The solid state structure of (a) [Ir(sacac)(cod)(CH_3)I] [29] and (b) the DFT optimized geometry [Ir(cupf)(cod)(CH_3)I]. Selected interatomic distances (Å) are shown to highlight the methyl group (NOESY) of the oxidative addition product and the proton(s) of the double bond of cod. Non H and C atoms are indicated with symbols and the hydrogens with a small black dot.

even number (positive mode) of protons. The ^{1}H–^{1}H NOESY experiment indicates strong coupling between the methyl of the oxidative addition product at δ 3.01 and the proton of the double bond of cod at δ 4.39, establishing that the methyl group is adjacent to these two protons. The HMBC experiment also confirmed long-range coupling between the oxidative addition methyl at δ 3.01 and the protons with the cyclooctadiene double bonds. Close inspection of the crystal structure of [Ir(sacac)(cod)(CH_3)I] [29] confirmed that the orientation of one of the methyl protons is in the direction of the cod C–C bond with the two $H_{(methyl)}$–$H_{(double\ bond)}$ interactions almost equal to each other (3.006 and 3.013 Å, respectively) endorsing that long-range coupling was observed (figure 3). This result is consistent with *trans* addition of CH_3I to [Ir(cupf)(cod)], similar to what was found for the oxidative addition product of CH_3I to [Ir(sacac)(cod)] [29].

Surprisingly the [Ir(tfaa)(cod)(CH_3)I] ^{13}C NMR spectrum shows the presence of only 10 of the 14 carbons in the product, which corroborates the nine carbons (instead of 13) observed for [Ir(tfaa)(cod)] as starting complex. This observation suggests, as was observed with the ^{1}H NMR spectrum, that the chemical environment changes insignificantly before and after oxidative addition, producing four equivalent cod carbons and therefore fewer carbons than expected. The APT experiment indicates seven carbons with an even number of protons

and three carbons with an odd number of protons, as expected for the methine and the two methyl groups in the final product. The NOESY experiment indicates a diagonal interaction between the new methyl group at δ 2.23 and two indistinguishable protons of the double bond at δ 4.29. The HMBC experiment confirms long-range coupling/interaction between the oxidative addition methyl group and a proton for one of the double bonds in cyclooctadiene.

The ^{13}C NMR spectrum of [Ir(macsm)(cod)(CH_3)I] showed the presence of 17 carbons in the oxidative product, while the APT experiments showed 10 carbons with odd number of protons, and 7 carbons with an even number of protons (positive mode). ^{1}H–^{1}H NOESY indicated diagonal interaction between the methyl group at δ 2.46 of the oxidative addition product and the proton of the double bonds at δ 4.98 and 5.63, which was confirmed with HMBC. The NOESY coupling between the methyl group of the oxidative addition product and the proton of the double bonds for [Ir(tfaa)(cod)CH_3I] and [Ir(macsm)(cod)(CH_3)I] indicates that the CH_3 groups are above the square plane of the Ir(I) complex.

The cod protons at 1.4–5.7 ppm compares favorably with those obtained for [Ir(triazalato)(cod)] (triazolato = 3.5-bis(pyridine-2-yl)-1,2,4 triazolate (bpt-NH) and 4-amino-3,5-bis(pyridine-2-yl)-1,2,4 triazolate (bpt)) [30], and [Ir(S,O)(cod)] (S,O = N-methyl-p-methoxybenzathiohydroxaminato and 1-hydroxi-2-pyridinato ligands) [31], which were observed between 1.8 and 3.8, and 1.7 and 4.4 ppm, respectively.

3.2. Kinetics

The initial UV/Vis scans after the addition of CH_3I confirm that the three complexes react with methyl iodide. The isolation of the products in acetone clearly indicates formation of only one product, the Ir(III) alkyl product according to scheme 1. The kinetic results for all of the oxidative addition reactions between CH_3I and the different complexes in acetonitrile showed simple second-order kinetics with zero intercepts for macsm and tfaa. The small intercept observed for the reaction between CH_3I and [Ir(cupf)(cod)] can either be a reversible or a parallel reaction (table 1). Only two possible reactions can occur parallel to the main oxidative addition, namely a solvent reaction with the square planar complex followed by the reaction of the solvated complex with the CH_3I to form the final oxidative addition complex or oxidative addition via a *cis* mechanism which differs in reaction rates. A solvent reaction pathway is highly unlikely since all the complexes were very stable in the different solvents (paragraph 2.1). DFT calculations (paragraph 3.3) predict two different approaches of CH_3I to the metal complex ("linear" or "bent") which both lead to *trans* addition while a "front" addition leads to *cis* addition. Interestingly the DFT calculations predict *cis* products for [Ir(cupf)(cod)] which have energy very similar to that of the *trans* product, but the activation energies of the "linear" (*trans* addition) and "front" (*cis* addition) transition states indicate that the "linear" transition state is energetically favored above the "front" transition, making *cis* addition highly unlikely. The intercept observed for the [Ir(cupf)(cod)] is therefore regarded as a reversible reaction and not a parallel reaction. The rate of oxidative addition for [Ir(macsm)(cod)] was the fastest (2.84(7) $\times$ 10^{-3} M s^{-1}) of the three complexes and larger by a factor 4 and 13 than [Ir(cupf)(cod)] and [Ir(tfaa)(cod)], respectively. The large negative entropy of activation indicates associative activation during the transition state. The forward reaction for [Ir(cupf)(cod)] is entropy controlled while the reverse reaction is enthalpy controlled.

Table 3. Summary of the kinetic data for the oxidative addition reactions between [Ir(LL)(cod)] and CH_3I in different solvents and bidentate ligands with different ring sizes at 25° C.

Complex	Donor atoms	Ring size	k_1 ($\times 10^2$) (M^{-1} s^{-1})	Solvent	Ref.
[Ir(macsm)(cod)]	S,N	6	2.84(7)	Acetonitrile	This study
[Ir(sacac)(cod)]	S,O	6	0.52(3)	Acetonitrile	[20]
[Ir(tfaa)(cod)]	O,O	6	0.44(2)	Acetonitrile	This study
[Ir(cupf)(cod)]	O,O	5	0.298(4)	Acetonitrile	This study
[Ir(AnMetha)(cod)]	S,O	5	2.69(6)	Nitromethane	[31]
[Ir(hpt)(cod)]	S,O	5	2.2(2)	Nitromethane	[31]
[Ir(bpt-NH)(cod)]	N,N	6	1.44(7)	Dichloromethane	[30]
[Ir(AnMetha)(cod)]	S,O	5	0.943(10)	Acetone	[31]
[Ir(hpt)(cod)]	S,O	5	0.693(17)	Acetone	[31]
[Ir(bpt)(cod)]	N,N	5	0.35(1)	Acetone	[30]
[Ir(bpt-NH)(cod)]	N,N	6	0.0919(4)	Benzene	[30]

A comparison of the rate of oxidative addition for the different complexes (table 3) in acetonitrile indicates the order N,S > S,O [20] > O,O for the bidentate donors, which corresponds favorably with the oxidative addition order of N,S > N,O > S,O > O,O [32] observed for a number of [Rh(LL′)(CO)(PPh_3)] complexes containing different donor combinations (LL′ = bidentate ligand of charge −1 and with donor L and L′). This increase in the oxidative addition rate is attributed to an increase in the nucleophilicity of the metal complex as a result of the better σ-bonding properties of nitrogen and sulfur compared to oxygen. A comparison with [Ir(bpt-NH)(cod)] [30] (triazolato complexes) may be questionable since the reactions were performed in different solvents than in the current study (dichloromethane and benzene); however, it is evident that the oxidative addition rate of this complex is in the same order of magnitude ($1.44(7) \times 10^{-2}$ M^{-1} s^{-1} in dichloromethane) as those in the current study.

DFT calculations for [M(triazolato)(cod)] [30] (M = Ir(I) and Rh(I)) predicted *cis* methyl iodide addition compared to the *trans* addition to [Ir(sacac)(cod)] and [Ir(acac)(cod)], which was also experimentally confirmed by the respective crystal structure determinations [29, 33]. A change in transition state and therefore a different final product is not surprising if the substantial steric interaction between the cod protons and the methyl group is taken into account, which is evident from the large deviation from linearity for the *trans* addition products. The similarity between the tfaa and sacac/acac and to a certain extent macsm, however, renders the above-mentioned argument questionable and more research is needed to conclusively prove or disprove the argument.

3.3. Computational chemistry

No solid state X-ray data on the geometry of [Ir(cupf)(cod)], [Ir(tfaa)(cod)] and [Ir(macsm)(cod)] are available [34], only powder diffraction data of [Ir(tfaa)(cod)] [35]. Thus, to get more insight into the structure of the iridium(I) cod complexes of this study, DFT computational chemistry was done to determine the optimized minimum energy geometries of [Ir(cupf)(cod)], [Ir(tfaa)(cod)], and [Ir(macsm)(cod)], as well as the iridium(III) products of oxidative addition of these complexes. Different views of the DFT optimized geometries of the [Ir(LL′)(cod)] complexes are shown in figure 4. The pseudo aromatic ring formed by Ir and the LL′-ligand is near planar in all three structures with a dihedral angle of −5.8° (SCCN in cupf), −0.2° (OCCO in tfaa), and −1.3° (ONNO in macsm). The two C=C bonds of cod are nearly

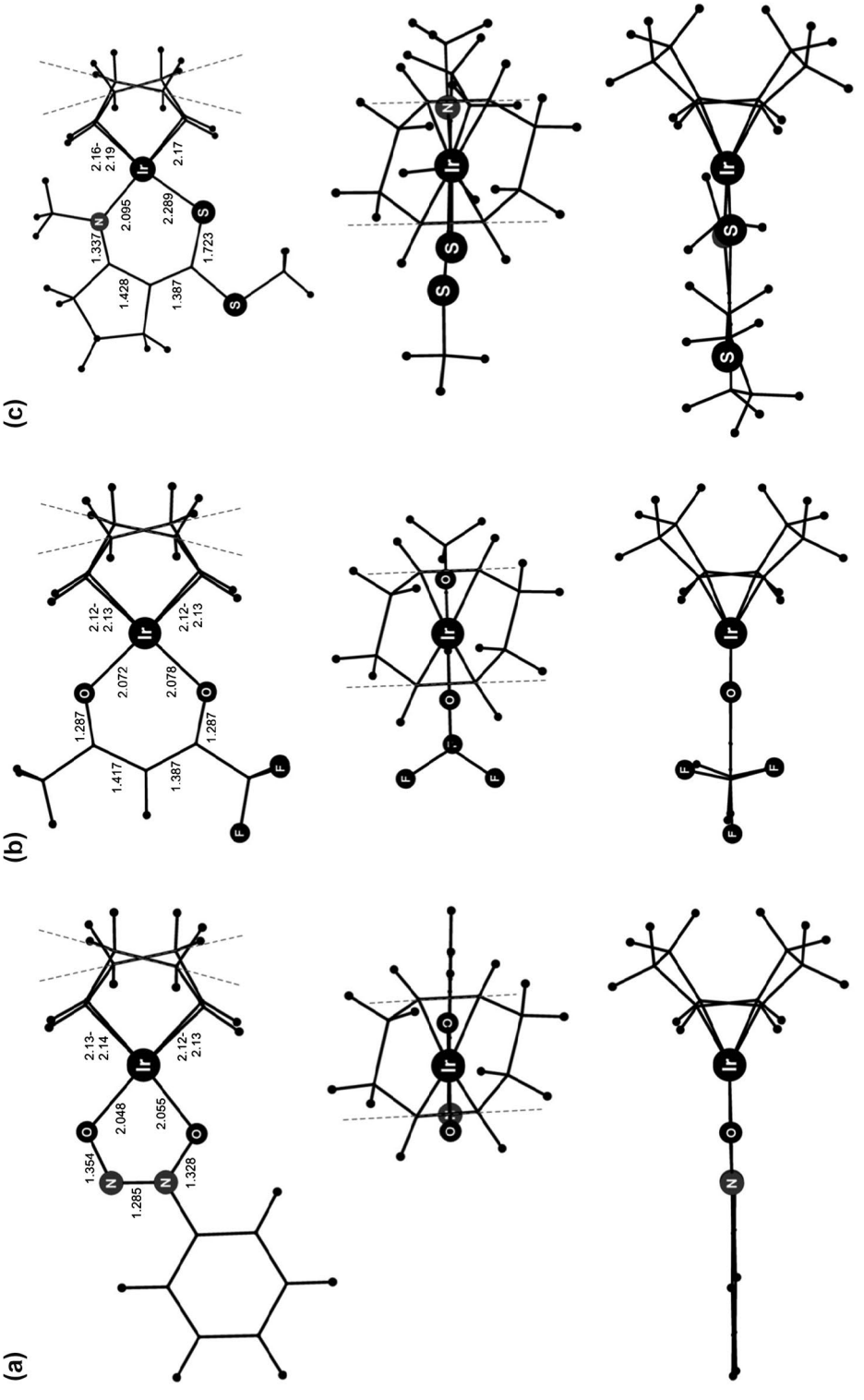

Figure 4. Three different views of the PW91/TZP optimized geometries of (a) [Ir(cupf)(cod)], (b) [Ir(tfaa)(cod)] and (c) [Ir(macsm)(cod)]. Selected bond lengths (Å) are indicated. The dotted gray lines in the top structures highlight the staggered conformation of the two CH_2CH_2– moieties of the cod ligand. The dotted gray lines in the middle structures highlight the nearly parallel conformation of the two C=C bonds of the cod ligand. Non H and C atoms are indicated with symbols and the hydrogens with a small black dot.

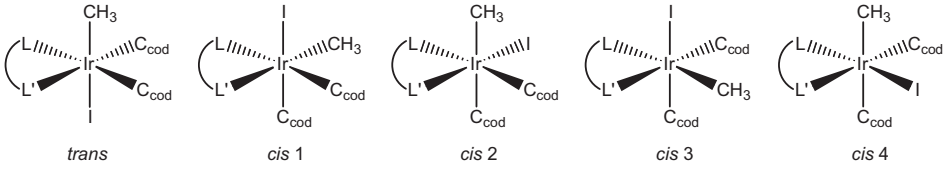

Scheme 3. Schematic illustrations of the *trans* and *cis* isomers of [Ir(LL')(CH_3)(I)(cod)].

Table 4. PW91/TZP DFT calculated electronic (E), enthalpy (H), and Gibbs free (G) energies (kJ mol^{-1}) of the possible transition states (TS) and possible products of the [Ir(LL')(cod)] + CH_3I oxidative addition reaction, relative to the energy of the reactants as 0.

	[Ir(cupf)(cod)]			[Ir(tfaa)(cod)]			[Ir(macsm)(cod)]		
	ΔE	ΔH	$\Delta G^{298\,K}$	ΔE	ΔH	$\Delta G^{298\,K}$	ΔE	ΔH	$\Delta G^{298\,K}$
Ir(I) + CH_3I	0.0	0.0	0.0	0.0	0.0	0.0	0.0	0.0	0.0
Ir(III)-alkyl *cis* 1	−55.0	−47	11.8	−54.8	−42	5.9	−7.3	2	52.1
Ir(III)-alkyl *cis* 2	−17.7	−9	40.5	−16.8	−8	43.2	−2.0	6	56.5
Ir(III)-alkyl *cis* 3	−50.9	−43	14.9	−56.3	−46	7.4	−10.1	−1	48.4
Ir(III)-alkyl *cis* 4	−21.0	−12	38.7	−16.6	−8	43.8	13.5	23	65.0
Ir(III)-alkyl *trans*	−49.8	−39	12.9	−60.8	−47	0.5	−45.0	−35	13.5
TS *front*	605.7	570	621.0	142.3	147	189.3	195.3	193	241.3
TS *trans*	29.0	31 (31 exp)	82.5 (87 exp)	29.8	35 (37 exp)	77.8 (86 exp)	27.6	29 (30 exp)	80.0 (82 exp)

parallel when coordinated to Ir, while the two CH_2CH_2- moieties of cod adopt a staggered conformation. The Ir-C_{cod} bonds are slightly longer (*ca.* 0.04 Å) in [Ir(macsm)(cod)] than in [Ir(cupf)(cod)] and [Ir(tfaa)(cod)]. The Ir-O bonds in [Ir(cupf)(cod)] with the more strained five-membered ring are slightly shorter (0.02–0.03 Å) than in [Ir(tfaa)(cod)] with a six-membered ring.

Oxidative addition of methyl iodide to [Ir(LL')(cod)] leads to an iridium(III) alkyl complex [Ir(LL')(CH_3)(I)(cod)]. The CH_3 group and I in [Ir(LL')(CH_3)(I)(cod)] can either be *trans* (*trans* product) or *cis* to each other (*cis* product). Four *cis* isomers are possible when the LL'-bidentate ligand is unsymmetrical (scheme 3). The relative energies of the optimized geometries of the five [Ir(LL')(CH_3)(I)(cod)] isomers for LL' = cupf, tfaa and macsm are given in table 4. The *trans* isomers have the lowest energies (most stable) for LL' = tfaa and macsm, while for LL' = cupf the energy of the *cis* 1, *cis* 3 and *trans* isomers are very near to each other.

Both experimental and theoretical data strongly support the S_N2 mechanism for the oxidative addition of methyl iodide to square planar complexes [36]. During the S_N2 attack, the methyl iodide can either approach the metal center in a linear way with the iodine directed away from the metal (leading to a "linear" transition state), or with C-I bond in a side-ways fashion (leading to a "bent" transition state) [37]. Both the "linear" and "bent" transition states lead to a five-coordinate methyl complex (of which the charge increases by 1) and a free iodide ion (of charge –1). After coordination of the iodide, a *trans* oxidative addition complex is formed [37]. A *cis* oxidative addition complex results from a "front" transition state (TS) where the C–I bond of methyl iodide also approaches the metal center in a side-ways fashion,

but then leads to a concerted three-center oxidative addition with simultaneous metal-I and metal-C formation and I-C breaking [37].

The calculated activation energies of the "linear" and "front" transition states for the oxidative addition reaction [Ir(LL')(cod)] + CH_3I for LL' = cupf, tfaa and macsm is given in table 4. No "bent" transition state could be located. The "linear" transition state is energetically favored, while the activation barrier of the "front" transition state is too high to occur. *Trans* [Ir(LL')(CH_3)(I)(cod)] products are thus formed for all three complexes of this study, including LL' = cupf where the energy of the *cis* 1 and *cis* 3 isomers are slightly lower than the energy of the *trans* isomer. This result is in agreement with computational chemistry and experimental results [20] for the related oxidative addition reaction [Ir(LL')(cod)] + CH_3I for LL' = sacac (sacac = thioacetyl acetonato), which was found to proceed through a "linear" transition state giving *trans*-[Ir(cod)(sacac)(CH_3)(I)] in the solid state [29]. The NMR results of the oxidative addition products, presented in a previous section, are also consistent with *trans* oxidative addition products for the three complexes of this study.

The optimized *trans*-[Ir(LL')(CH_3)(I)(cod)] products have a distorted octahedral structure with the I–Ir–CH_3 angle (156–158°) deviating from linearity, possibly due to steric repulsion between the CH_3 or I and the olefinic hydrogens (figure 5). These results correlate very well with the experimentally obtained I–Ir–CH_3 bond angles of 156.06° and 156.58°, which were reported for [Ir(cod)(sacac)(CH_3)(I)] and [Ir(cod)(acac)(CH_3)(I)] [33]. The optimized geometries of the "linear" transition state of the [Ir(LL')(cod)] + CH_3I oxidative addition of each complex are shown in figure 6. During the "linear" transition state of the oxidative addition process, iridium approaches the methyl iodide *trans* to the leaving iodide with formation of the

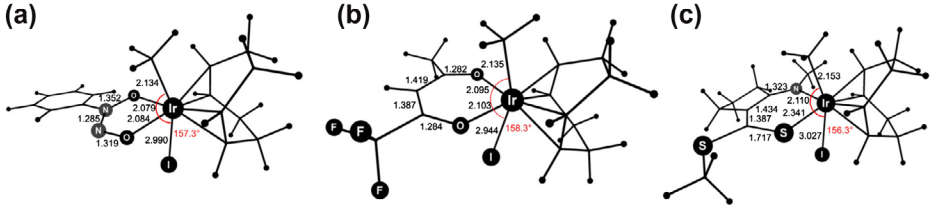

Figure 5. PW91/TZP optimized geometries of the *trans* oxidative addition product of [Ir(LL')(cod)] + CH_3I oxidative addition reaction for LL' = (a) cupf, (b) tfaa, and (c) macsm. Selected bond lengths (Å) and angles (deg) are indicated. Non H and C atoms are indicated with symbols and the hydrogens with a small black dot.

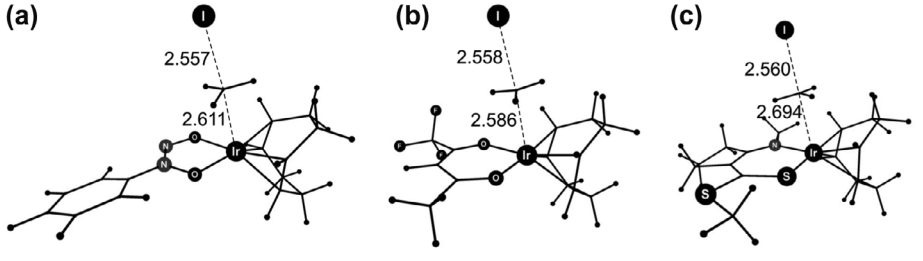

Figure 6. PW91/TZP optimized geometries of the *linear* transition state of [Ir(LL')(cod)] + CH_3I oxidative addition reaction for LL' = (a) cupf, (b) tfaa, and (c) macsm. Selected bond lengths (Å) are indicated. Non H and C atoms are indicated with symbols and the hydrogens with a small black dot.

Ir-methyl bond and simultaneous dissociation of the Me-I bond. The methyl iodide is tilted towards LL′-bidentate ligand, probably due to steric influence of the cod ligand. The computational chemistry calculated activation free energy of the "linear" transition state is in good agreement with experimental values (table 4). The DFT calculated enthalpy values in table 4 show that the oxidative addition reaction is exothermic, the product Ir(III)-alkyl *trans* is 35–47 kJ mol^{-1} more stable than the separate reactants, CH_3I and the Ir(I) complex. DFT calculated large negative activation entropy values (−172, −145 and -170 J K^{-1} mol^{-1} for [Ir(cupf)(cod)], [Ir(tfaa)(cod)], and [Ir(macsm)(cod)], respectively) indicate an associative activation during the transition state.

4. Conclusion

We have synthesized three different [Ir(LL′)(cod)] complexes (LL′ = N-aryl-N-nitrosohydroxylaminato) (cupf), trifluoroacetylacetonato (tfaa) and (methyl 2-(methylamino)-1-cyclopentene-1-dithiocarboxylato-κN, κS) (macsm)). All the complexes were characterized by ^1H and ^{13}C NMR spectroscopy, IR, elemental microanalysis, and mass spectrometry. Their rates of oxidative addition with methyl iodide were determined. The computational study of [Ir(LL′)(cod)] + CH_3I oxidative addition reaction for LL′ = cupf, tfaa and macsm, in agreement with ^1H NMR results, showed that the oxidative addition reaction proceeds through a "linear" transition state with a calculated activation energy in agreement with experimental values. The transition state corresponds to a S_N2 nucleophilic attack by the metal compound on methyl iodide. A concerted three center "front" transition state structure exists as well, but is not energetically favored.

Disclosure statement

No potential conflict of interest was reported by the authors.

Funding

This work was supported by the Norwegian Supercomputing Program (NOTUR) through a grant of computer time [grant number NN4654 K] (JC); the South African National Research Foundation; and the Central Research Fund of the University of the Free State, Bloemfontein, South Africa.

References

[1] T.W. Dekleva, D. Foster. *Adv. Catal.*, **34**, 81 (1986).
[2] A. Haynes, P.M. Maitlis, G.E. Morris, G.J. Sunley, H. Adams, P.W. Badger, C.M. Bowers, D.B. Cook, P.I.P. Elliott, T. Ghaffar, H. Green, T.R. Griffin, M. Payne, J.-M. Pearson, M.J. Taylor, P.W. Vickers, R.J. Watt. *J. Am. Chem. Soc.*, **126**, 2847 (2004).
[3] P.M. Maitlis, A. Hayes, G.J. Sunley, M.J. Howard. *J. Chem. Soc., Dalton Trans.*, 2187 (1996). doi: 10.1039/DT9960002187.
[4] P.D. Pavlechko, IHS Chemical Report, Review (2103). Available online at: www.ihs.com/pdf/RW2014-01_toc_183772110917062932.pdf (accessed 16 March 2015).
[5] H-U. Blaser. *Adv. Synth. Catal.*, **344**, 17 (2002).
[6] H.-U. Blaser, B. Pugin, F. Spindler, M. Thommen. *Acc. Chem. Res.*, **40**, 1240 (2007).
[7] R. Dorta, D. Broggini, R. Stoop, H. Rüegger, F. Spindler, A. Togni. *Chem. Eur. J.*, **10**, 267 (2004).
[8] R.H. Crabtree. *Acc. Chem. Res.*, **12**, 331 (1979).

[9] R.H. Crabtree, H. Felkin, T. Fillebeen-Khan, G.E. Morris. *J. Organomet. Chem.*, **168**, 183 (1979).
[10] J.M. Bueno, J.M. Coterón, J.L. Chiara, A. Fernández-Mayoralas, J.M. Fiandor, N. Valle. *Tetrahedron Lett.*, **41**, 4379 (2000).
[11] S. Hietkamp, D.J. Stufkens, K. Vrieze. *J. Organomet. Chem.*, **139**, 189 (1977).
[12] G. Winkhuis, H. Singer. *Z. Naturforsch., Teil B*, **20**, 602 (1965).
[13] M. Green, T.A. Kuc, S.H. Taylor. *J. Chem. Soc., A*, 2334 (1971).
[14] S. Hietkamp, D.J. Stufkens, K. Vrieze. *J. Organomet. Chem.*, **122**, 419 (1976).
[15] J.-Y. Chen, J. Halpern. *J. Am. Chem. Soc.*, **93**, 4939 (1971).
[16] D. Astruc. *Organometallic Chemistry and Catalysis*, p. 435, Springer Heidelberg Berlin, New York (2000).
[17] J.G. Leipoldt, E.C. Steynberg, R. Van Eldik. *Inorg. Chem.*, **26**, 3068 (1987).
[18] J.A. Venter, J.G. Leipoldt, R. Van Eldik. *Inorg. Chem.*, **30**, 2207 (1991).
[19] (a) M.M. Conradie, J. Conradie. *Inorg. Chim. Acta*, **361**, 208 (2008); (b) M.M. Conradie, J. Conradie. *Inorg. Chim. Acta*, **361**, 2285 (2008); (c) N.F. Stuurman, J. Conradie. *J. Organomet. Chem.*, **694**, 259 (2009); (d) M.M. Conradie, J. Conradie. *Inorg. Chim. Acta*, **362**, 519 (2009).
[20] W. Purcell, J. Conradie, S. Kumar, J.A. Venter. *J. Organomet. Chem.*, **801**, 80 (2016).
[21] D.D. Perrin, W.L.F. Armarego. *Purification of Laboratory Chemicals*, 3rd Edn, Pergamon Press, Oxford (1988).
[22] *Scientist*, Version 2, MicroMath Scientific Software, St. Louis, MO (2004).
[23] B. Bordas, P. Sohar, G. Matolcsy, P. Berencsi. *J. Org. Chem.*, **37**, 1727 (1972).
[24] ADF2013, SCM, Theoretical Chemistry, Vrije Universiteit, Amsterdam, The Netherlands, The ADF program system uses methods described in: G. teVelde, F.M. Bickelhaupt, E.J. Baerends, C.F. Guerra, S.J.A. van Gisbergen, J.G. Snijders, T. Ziegler. *J. Comput. Chem.*, **22**, 931 (2001).
[25] (a) J.P. Perdew, J.A. Chevary, S.H. Vosko, K.A. Jackson, M.R. Pederson, D.J. Singh, C. Fiolhais. *Phys. Rev. B*, **46**, 6671 (1992); (b) Erratum: J.P. Perdew, J.A. Chevary, S.H. Vosko, K.A. Jackson, M.R. Pederson, D.J. Singh, C. Fiolhais. *Phys. Rev. B*, **48**, 4978 (1993).
[26] (a) E. van Lenthe, A. Ehlers, E.J. Baerends. *J. Chem. Phys.*, **110**, 8943 (1999); (b) E. van Lenthe, E.J. Baerends, J.G. Snijders. *J. Chem. Phys.*, **99**, 4597 (1993); (c) E. van Lenthe, E.J. Baerends, J.G. Snijders. *J. Chem. Phys.*, **101**, 9783 (1994); (d) E. van Lenthe, J.G. Snijders, E.J. Baerends. *J. Chem. Phys.*, **105**, 6505 (1996); (e) E. van Lenthe, R. van Leeuwen, E.J. Baerends, J.G. Snijders. *Int. J. Quantum Chem.*, **57**, 281 (1996).
[27] (a) A. Klamt, G. Schüürmann. *J. Chem. Soc., Perkin Trans. 2*, **799**, (1993); (b) A. Klamt. *J. Phys. Chem.*, **99**, 2224 (1995); (c) A. Klamt, V.J. Jonas. *J. Chem. Phys.*, **105**, 9972 (1996).
[28] J.L. Pascual-ahuir, E. Silla, I. Tuñon. *J. Comput. Chem.*, **15**, 1127 (1994).
[29] Y.M. Terblans, S.S. Basson, W. Purcell, G.J. Lamprecht. *Acta Crystallogr., Sect. C*, **51**, 1748 (1995).
[30] A. Muller, J. Conradie, W. Purcell, S.S. Basson, J.A. Venter. *S. Afr. J. Chem.*, **63**, 11 (2010).
[31] M. Theron, E. Grobbelaar, W. Purcell, S.S. Basson. *Inorg. Chim. Acta*, **358**, 2457 (2005).
[32] (a) A. Roodt, G.J.J. Steyn. *Recent Research Developments in Inorganic Chemistry*, **2**, 1 (2000); (b) J.G. Leipoldt, S.S. Basson, L.J. Botha. *Inorg. Chim. Acta*, **168**, 215 (1990).
[33] S.S. Basson, J.G. Leipoldt, W. Purcell, J.B. Schoeman. *Acta Cryst. C*, **45**, 2000 (1989).
[34] Cambridge Structural Database (CSD), Version 5.36, May 2015 update.
[35] L. Davignon, A. Dereigne, R. Bonnaire, J.M. Manoli. *J. Less Common Met.*, **25**, 75 (1971).
[36] (a) T.R. Griffin, D.B. Cook, A. Haynes, J.M. Pearson, D. Monti, G.E. Morris. *J. Am. Chem. Soc.*, **118**, 3029 (1996); (b) M.M. Conradie, J. Conradie. *Dalton Trans.*, **40**, 8226 (2011).(c) J.J.C. Erasmus, J. Conradie. *Dalton Trans.*, **42**, 8655 (2013); (d) M.M. Conradie, J. Conradie. *J. Organomet. Chem.*, **695**, 2126 (2010); (e) M.M. Conradie, J. Conradie. *S. Afr. J. Chem.*, **61**, 102 (2008). Available online at: http://www.journals.co.za/sajchem/.
[37] M. Feliz, Z. Freixa, P.W.N.M. van Leeuwen, C. Bo. *Organometallics*, **24**, 5718 (2005).